Role of the inter-sublattice exchange coupling in short-laser-pulse-induced demagnetization dynamics of GdCo and GdCoFe alloys

A. Mekonnen,[1,*] A. R. Khorsand,[1] M. Cormier,[1] A. V. Kimel,[1] A. Kirilyuk,[1] A. Hrabec,[2] L. Ranno,[2]
A. Tsukamoto,[3] A. Itoh,[3] and Th. Rasing[1]

[1]*Radboud University Nijmegen, Institute for Molecules and Materials, Heyendaalseweg 135, 6525 AJ Nijmegen, The Netherlands*
[2]*Institut Néel, CNRS/UJF, 25 Rue des Martyrs, 38042 Grenoble Cedex 9, France*
[3]*College of Science and Technology, Nihon University, 7-24-1 Funabashi, Chiba, Japan*

The dynamics of the demagnetization induced by an ultrashort laser pulse in GdCo and GdCoFe alloys is shown to be substantially different from the expected trend. We find that the intersublattice exchange interaction between Gd and Co(Fe) is used as an additional route of heat transfer during the demagnetization process and leads to a temporary cooling of the Co(Fe) spin subsystem. The observed results are described by a four-temperature model (4T model) in which electrons, lattice, and $4f$ and $3d$ spins represent four reservoirs of heat energy. In this model, the coupling between the electron and spin reservoirs is responsible for an ultrafast demagnetization, while the intersublattice exchange coupling gives rise to an immediate remagnetization and serves as a thermal link between the Co(Fe) and Gd spins.

The interaction of a subpicosecond optical laser pulse with spins in a magnetic system has become a rapidly growing area of science[1–11] since the pioneering work by Beaurepaire *et al*. Using a 60 fs optical laser pulse, they demonstrated an ultrafast (within about 1 ps) demagnetization in a Ni thin film.[1] After this observation, research on laser-induced demagnetization has been conducted at large in ferromagnetic transition metals (TMs) (e.g., Co, Ni), rare-earth (RE) metals (e.g., Gd, Tb), and their alloys (see Ref. 12 and references therein). From a technological point of view, the possibility of manipulating spins on the time scale of a few picoseconds with a short optical laser pulse has great potential for designing faster spintronic and magnetic data-storage devices.

The response of the RE moments upon optical-laser-pulse perturbation is different from that of the TM moments. This is because the magnetism in the RE metals mainly originates from the deeply buried $4f$ localized electrons, while the magnetism in the TMs originates from the $3d$ delocalized conduction electrons. As a result, the magneto-optical signal of the RE metals is much smaller than that of TMs in the (near) infrared regime.[13–15] For instance, it has been reported that Gd shows a three-order-of-magnitude slower demagnetization time than Co.[3,4,10] Moreover, recently it has been shown that Gd also shows a partial ultrafast demagnetization process[8,11] in addition to the dominant slower demagnetization. Regardless of the above-mentioned differences between TMs and RE metals, it was generally accepted up to now that the demagnetization dynamics in RE-TM alloys induced by an optical laser pulse was an ultrafast process.[5,16] Such results were described by the standard three-temperature model (3T model).[1,10,17]

In this Rapid Communication, we show that the dynamics induced by an ultrashort laser pulse in GdCo and GdCoFe shows a three-step demagnetization process, which is different from the demagnetization trend expected from the conventional 3T model. Instead we propose a phenomenological four-temperature model (4T model) to describe the laser-induced demagnetization processes in GdCo and GdCoFe.

The experimental observations are well explained by this 4T model, consisting of four coupled differential equations which take the heat flow between the different heat baths (electrons, lattice, and $4f$ and $3d$ spins) into consideration.

For the pump-probe magneto-optical–Kerr-effect measurement, we used an amplified-pulsed Ti:sapphire laser at a wavelength of 800 nm, with a repetition rate of 1 kHz and a pulse width of about 100 fs. After splitting the beam into two linearly polarized parts with unequal power, the stronger pump pulse incident at $30°$ from the sample normal was focused to a spot diameter of around 400 μm, while the weaker probe pulse incident at $45°$ from the sample normal, controllably delayed, was focused to a smaller spot diameter which was around 85 μm. The larger spot size of the pump over the probe beam ensures homogeneous heating in the probed area of the sample. The magnetization was locked along its easy direction by an external magnetic field, the magnitude of which was greater than the coercive field. The present experimental geometry at room temperature avoids laser-induced magnetization precessions[18] as well as laser-induced switching across a ferrimagnetic compensation point.[19–21] Rather, we are sensitive to the out-of-plane magnetization change as a result of laser-induced heating. Note that in the experiment, the magneto-optical signal of GdCo(Fe) comes mainly from the Co(Fe) $3d$ moments.[13,14] This is because the $4f$ moments of Gd are deeply buried with a potential energy of about -8.4 eV,[22] while the used photon energy is ≈1.5 eV. The magnetic moments of the Co(Fe) and Gd sublattices couple antiparallel to each other via a strong intersublattice $3d$-$5d6s$-$4f$ exchange interaction, which is responsible for the ferrimagnetism of the alloy. As a result of this strong exchange coupling, such alloys are known to have a high Curie temperature (T_C) that is common for the two sublattices.[17,23,24]

First we used an amorphous $Gd_{17}Co_{83}$ ferrimagnetic thin film, grown by magnetron sputtering on a quartz substrate and sandwiched in between two Ti layers: Ti(3 nm)/$Gd_{17}Co_{83}$(20 nm)/Ti(3 nm)/quartz.[20] This alloy has
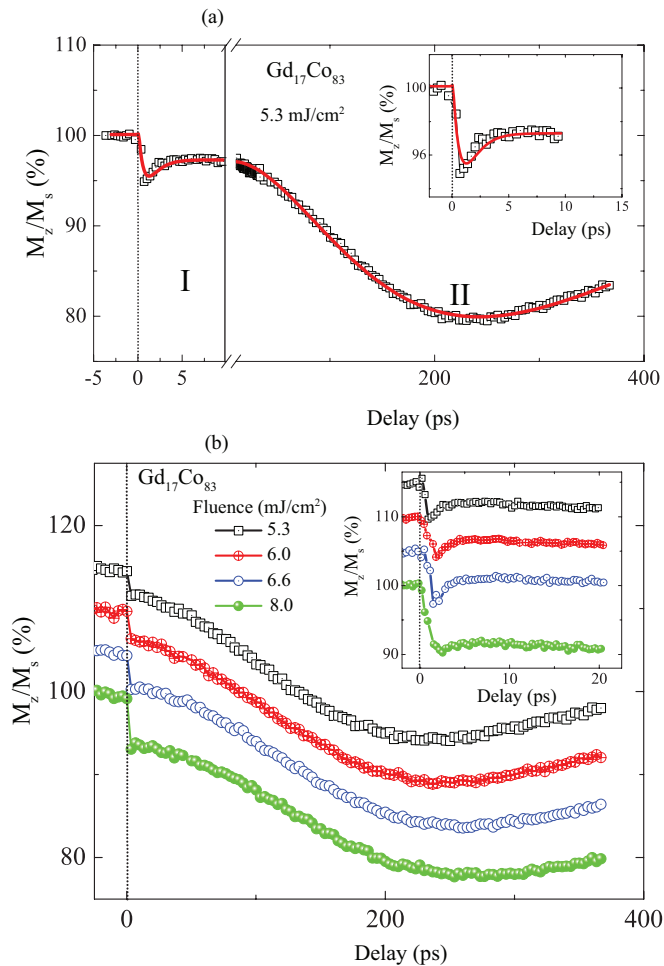
FIG. 1. (Color online) (a) Laser-pulse-induced demagnetization dynamics in $Gd_{17}Co_{83}$ using a pump-laser fluence of 5.3 mJ/cm². A partial ultrafast demagnetization (regime I) followed by an immediate recovery (remagnetization), and a dominating slower demagnetization (regime II) are observed. The solid curves are fits using biexponential functions, while the vertical dotted line represents the zero delay between pump and probe pulses. (b) Demagnetization dynamics as a function of pump-laser fluence. The insets show a zoom-in of the faster demagnetization process.

an out-of-plane magnetic anisotropy and a very high $T_C \approx$ 900 K.[23,24]

The results of a time-resolved demagnetization measurement in $Gd_{17}Co_{83}$ using a pump-laser fluence of 5.3 mJ/cm² are presented in Fig. 1(a) (the vertical dotted line represents the overlap point of pump and probe pulses). Surprisingly, three magnetization features were observed. These are (i) a partial (a few %) ultrafast demagnetization process within the first picosecond after the pump pulse, (ii) a fast recovery (remagnetization) within a few picoseconds, and (iii) a dominating and slower demagnetization process which occurs in hundreds of picoseconds. To simplify the discussion, we classified the observed dynamics into two main regimes (regime I and regime II) [main panel in Fig. 1(a)]. The data in I and II were fitted separately by using biexponential functions [see the solid curves in Fig. 1(a)]. From the fitting curves, two characteristic

demagnetization time constants $\tau_{\text{dem}} = 700 \pm 200$ fs (I) and $\tau_{\text{dem}} = 123 \pm 5$ ps (II) have been extracted. In I, the magnetization reaches a minimum at $\approx$1–2 ps; after this time, the magnetization starts to recover and this process reaches its maximum at about 5 ps [see the inset in Fig. 1(a)]. Then, the second slower dominating demagnetization process follows. We have also performed similar measurements on the same sample as a function of pump-laser fluence [Fig. 1(b)]. The faster process is plotted as an inset. From these measurements, one can see that the amplitude of the ultrafast demagnetization increases with increasing fluence.

The laser-induced demagnetization in GdCo shows some peculiar features: (i) stoichiometrically Co is the dominant sublattice and we are mainly detecting Co in our magneto-optical measurements; however, the observed effects deviate significantly from the expected demagnetization of pure Co, which shows a very fast demagnetization;[10] (ii) the magnetization recovers immediately after the partial ultrafast demagnetization before the slower secondary demagnetization process starts; this was not previously observed in demagnetization studies of pure Co; (iii) because of the slower demagnetization feature, the observed laser-induced effect is similar to the demagnetization result of Gd, although the signal comes mainly from Co.

To get further insight in the laser-induced demagnetization processes observed in GdCo, and to verify whether the observed effects are unique to only the GdCo alloy or a general intrinsic property of multisublattice alloys, we have performed another set of measurements on an amorphous alloy with a different rare-earth transition-metal content, $Gd_{22}Co_{9.8}Fe_{68.2}$. The film was grown in the following multilayer structure: SiN(60 nm)/GdCoFe(20 nm)/SiN(5 nm)/AlTi(10 nm)/glass. The AlTi layer was used as a heat sink, whereas SiN was used as a buffer, capping, and antireflection coating. In this alloy, the Co and Fe sublattice magnetizations are coupled ferromagnetically with each other and the total magnetization of Fe and Co is coupled antiferromagnetically with that of Gd, yielding a ferrimagnetic order. This film also has an out-of-plane magnetic anisotropy. It has a lower Curie temperature, $T_C \approx 500$ K,[17,23] as compared to GdCo. The addition of Co in GdFe increases the magneto-optical signal and the T_C as compared to a pure GdFe alloy.

Under the same conditions as the experiments on GdCo presented in Fig. 1, we performed laser-induced demagnetization measurements on $Gd_{22}Co_{9.8}Fe_{68.2}$. Figure 2 shows the demagnetization obtained as a function of pump-laser fluence. Generally, a dominant ultrafast laser-induced demagnetization process is observed, which is consistent with previous studies,[5,16] and this process increases with pump-laser fluence. On the other hand, in agreement with the demagnetization observed in GdCo, the ultrafast demagnetization is followed by a recovery of the magnetization before a slower secondary demagnetization process follows (see the inset in Fig. 2).

Attempting to explain the laser-induced demagnetization dynamics of a ferrimagnetically coupled system with the standard 3T model requires one to assume that the global spin subsystem has only two energy-transfer channels, i.e., coupling with the electrons and lattice heat reservoirs. However, in RE-TM ferrimagnets, the RE and TM spins are fundamentally different[25] and they have distinct responses to
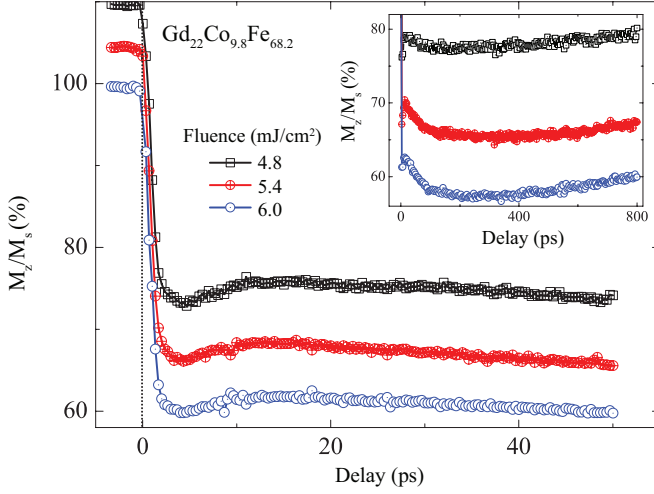
FIG. 2. (Color online) Laser-induced demagnetization as a function of pump-laser fluence in $Gd_{22}Co_{9.8}Fe_{68.2}$. The main panel shows the dynamics for short times, while the inset shows the one for longer times.

laser-pulse perturbation.[22,26] As a consequence, assigning one common spin subsystem (heat reservoir) and temperature for the two sublattices is not realistic. Therefore, we propose a phenomenological 4T model, which can be applied for a broad class of multisublattice systems, in which the spin systems of RE and TM are treated separately.

In the following, we take the GdCoFe alloy as a primary example. In this sample, a large percentage of the composition is Fe, thus we represent CoFe by Fe.

The Fe $3d$ spins and the Gd $4f$ spins are represented by two separate heat reservoirs. Note that the $4f$ and $5d6s$ spins of Gd are treated as a single spin subsystem, since they are strongly coupled via a strong (94 meV) intra-atomic $4f$-$5d6s$ exchange interaction.[27] The electrons and lattice common heat reservoirs are modeled in the same way as in the 3T model. Therefore, we end up with four different interacting heat reservoirs (see the Supplemental Material in Ref. 29). The 4T model can be represented by four coupled differential equations, which describe the heat flow between the heat reservoirs. These equations can be written as follows:

$$C_e(T_e)\frac{dT_e}{dt} = -G_{el}(T_e - T_l) - G_{es}^{Fe}(T_e - T_s^{Fe})$$
$$- G_{es}^{Gd}(T_e - T_s^{Gd}) + P(t),$$

$$C_l(T_l)\frac{dT_l}{dt} = -G_{el}(T_l - T_e) - G_{ls}^{Fe}(T_l - T_s^{Fe})$$
$$- G_{ls}^{Gd}(T_l - T_s^{Gd}),$$

$$C_s^{Fe}(T_s^{Fe})\frac{dT_s^{Fe}}{dt} = -G_{es}^{Fe}(T_s^{Fe} - T_e) - G_{ls}^{Fe}(T_s^{Fe} - T_l)$$
$$- G_{ss}^{Gd-Fe}(T_s^{Fe} - T_s^{Gd}),$$

$$C_s^{Gd}(T_s^{Gd})\frac{dT_s^{Gd}}{dt} = -G_{es}^{Gd}(T_s^{Gd} - T_e) - G_{ls}^{Gd}(T_s^{Gd} - T_l)$$
$$- G_{ss}^{Gd-Fe}(T_s^{Gd} - T_s^{Fe}),$$

where C_e and C_l are the electronic and lattice specific heats, and $C_s^{Fe,Gd}$ are the spin specific heats of the Fe and Gd sublattices, respectively. G_{el}, G_{es}^{Fe}, and G_{es}^{Gd} are electron-lattice and electron-spin (of Fe and Gd) coupling constants. $G_{ls}^{Fe,Gd}$ and G_{ss}^{Gd-Fe} are lattice-spin (of Fe and Gd) and spin-spin (between Fe and Gd sublattices) coupling constants.

A source $P(t)$, with a 100 fs full width at half maximum (FWHM) and with a peak power density of 2.5×10^{21} W/m^3, was applied to the electronic subsystem and, using typical parameters for Fe and Gd sublattices (details are provided in the Supplemental Material in Ref. 29), the four coupled differential equations were solved using a differential-equation solver based on the Runge-Kutta method. The result [Fig. 3(a)] shows that the electronic temperature T_e reaches about 890 K (not shown) within a time of about 100 fs, while $T_s^{Fe,Gd}$ and T_l remain close to room temperature. The heat deposited in the electronic subsystem is gradually redistributed to the spin and lattice subsystems. This process leads to an increase of the spin and lattice temperatures and a decrease of the electron temperature. As the delay increases, the lattice reaches thermal equilibrium with the electronic subsystem. However, an extraordinary dynamical feature (dip) is observed in the Fe spin temperature T_s^{Fe}. Following this, the two spin subsystems reach thermal equilibrium with each other and with the other subsystems at a much longer time (after 200 ps).

The dynamics of the Fe spin temperature T_s^{Fe} is discussed in three time windows [see Fig. 3(a)]: (i) $t_1 < 4$ ps, (ii) 4 ps $< t_2 < 10$ ps, and (iii) $t_3 > 10$ ps. Within $t_1 < 4$ ps, the temperature of the Fe spin reservoir T_s^{Fe} rapidly increases. In this regime, the dynamics of T_s^{Fe} is largely influenced by the electronic temperature because of the strong coupling between the Fe spin and electron subsystems. Therefore, an ultrafast laser-induced demagnetization process in Fe, controlled by the electronic temperature, occurs within this time window. However, within t_1, the temperature of the Gd spin reservoir T_s^{Gd} is still close to room temperature. Within t_2, the temperature of the electronic subsystem decreases and reaches a quasiequilibrium state with the phonon reservoir. From the third equation of the 4T model, we see that the term $-G_{ss}^{Gd-Fe}(T_s^{Fe} - T_s^{Gd})$ has a negative contribution to the slope of the Fe spin temperature, dT_s^{Fe}/dt. When this term is dominating over the other terms, T_s^{Fe} decreases, as shown in Fig. 3(a). It indicates that there is a heat flow from the Fe spins to the Gd spins (temporarily the Gd spin reservoir serves as a heat sink) via the intersublattice exchange coupling, which serves as a heat-transfer channel efficient within t_2. This result is in agreement with the computational work performed using an atomistic spin model.[17] Finally, for $t_3 > 10$ ps, we see that the spin temperatures of the Gd and Fe sublattices are steadily increasing.

An additional calculation was performed by neglecting the role of the Gd subsystem (putting $G_{ss}^{Gd-Fe} = G_{es}^{Gd} = G_{ls}^{Gd} = 0$); thus the 4T model is reduced to the 3T model. The resulting temporal evolution of the heat-reservoir temperatures [Fig. 3(b)] is very typical for pure $3d$ metals.[28]

To get a qualitative picture of the evolution of the magnetization, the temperature of each spin subsystem was mapped onto the corresponding magnetization by a simple Bloch $T^{3/2}$ law, that is, $M(T)/M(T_{room}) = [1 - (T/T_C)^{3/2}]$. We used $T_C = 500$ K for GdCoFe.[17] The normalized magnetizations of the Fe and Gd sublattices estimated from the 3T model and 4T
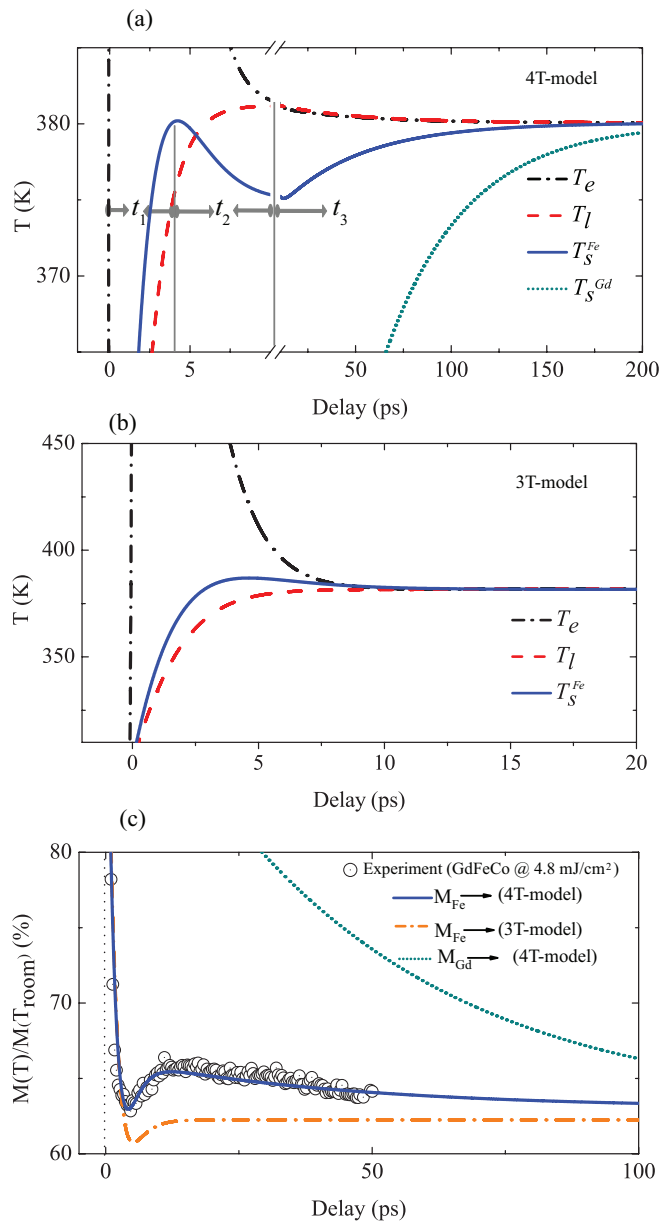
FIG. 3. (Color online) Numerically calculated curves that show (a) the temporal evolution of the heat-reservoir temperatures (T_e, T_l, T_s^{Fe}, and T_s^{Gd}) in GdCoFe within the 4T model (the calculation parameters are detailed in the Supplemental Material in Ref. 29), following the heating of the electronic subsystem. The two vertical solid lines indicate the boundaries of different time windows (t_1, t_2, and t_3). (b) The temporal evolution of the heat-reservoir temperatures (T_e, T_l, T_s^{Fe}) within the 3T model in pure Fe. (c) The magnetization change estimated by mapping the spin temperature onto the corresponding magnetization by a Bloch $T^{3/2}$ law. The expected demagnetization curve of pure Fe is reproduced using the 3T model (dash-dotted line). The demagnetization estimated from the 4T model is shown by the solid and dotted lines for Fe and Gd sublattices, respectively. The symbols represent the experimental demagnetization data of GdCoFe which was taken at 4.8 mJ/cm². The vertical dotted line represents the zero delay.

model are plotted in Fig. 3(c) (the vertical dotted line represents the zero delay). The one corresponding to the 3T model [dash-dotted line in Fig. 3(c)] shows the typical laser-induced

demagnetization expected for pure 3d metals.[10,28] On the other hand, the demagnetization process calculated from the 4T model [solid line in Fig.3(c)] shows a very good agreement with the experiment data obtained for GdCoFe (symbols). Therefore, from both the model and the experiment, one can conclude that the Gd sublattice is responsible for the odd feature of laser-induced demagnetization in GdCo and GdCoFe alloys.

From the experiment, we see that the ultrafast demagnetization is only partial in GdCo, whereas it is dominant in GdCoFe, which can be attributed to the differences between the two alloys. For instance, GdCo has, in general, a higher T_C than GdCoFe,[17,23,24] which implies a stronger intersublattice exchange interaction between TM and RE (spin-spin coupling). It is also shown that the slope of the remagnetization in GdCo is steeper than in GdCoFe (Figs. 1 and 2). This can be reproduced within the 4T model, where the steepness of the remagnetization can be controlled by the strength of the spin-spin coupling constant: the stronger the coupling, the steeper the remagnetization slope. This confirms the adequateness of the 4T model in explaining the laser-induced dynamics in both GdCo and GdCoFe alloys on the time scale of the exchange interaction. Further detailed comparison between the two alloys will be made in an upcoming paper.

In conclusion, using a time-resolved all-optical pump-probe magneto-optical–Kerr-effect experiment, the demagnetization dynamics of GdCo and GdCoFe ferrimagnetic thin films was investigated. In both alloys, two types of demagnetization processes have been revealed, i.e., an ultrafast demagnetization process which occurs on a subpicosecond time scale followed by an immediate remagnetization, and then a slower demagnetization process. Although the magnetism of Gd is not directly accessible in these magneto-optical measurements, its fingerprint is clearly visible on the demagnetization dynamics of Co(Fe) as a result of the intersublattice 3d-5d6s-4f exchange interaction. This interaction serves to couple the Co(Fe) and Gd spins heat baths and it is the driving force behind the immediate remagnetization observed after the partial ultrafast demagnetization. The experimental observations are explained using a four-temperature model, consisting of four coupled differential equations which take the heat flow between the different heat baths (electrons, lattice, and 4f and 3d spins) into consideration. These results clearly demonstrate the existence of an extra channel to control the laser-pulse-induced demagnetization process of TMs in ferrimagnetically coupled multisublattice systems, which represents a step forward in our understanding of all-optical manipulation of magnetization and may lead to the design of optimal materials for magnetic data storage.

*Corresponding author: addis@chalmers.se;
Present address: Chalmers University of Technology, Department of Applied Physics, 412 96 Göteborg, Sweden.

[1] E. Beaurepaire, J.-C. Merle, A. Daunois, and J.-Y. Bigot, Phys. Rev. Lett. **76**, 4250 (1996).

[2] W. Hübner and K. H. Bennemann, Phys. Rev. B **53**, 3422 (1996).

[3] A. Vaterlaus, T. Beutler, and F. Meier, Phys. Rev. Lett. **67**, 3314 (1991).

[4] A. Vaterlaus, T. Beutler, D. Guarisco, M. Lutz, and F. Meier, Phys. Rev. B **46**, 5280 (1992).

[5] J. Hohlfeld, T. Gerrits, M. Bilderbeek, T. Rasing, H. Awano, and N. Ohta, Phys. Rev. B **65**, 012413 (2001).

[6] L. Guidoni, E. Beaurepaire, and J.-Y. Bigot, Phys. Rev. Lett. **89**, 017401 (2002).

[7] A. Bartelt, A. Comin, J. Feng, J. Nasiatka, T. Eimüller, B. Ludescher, G. Schütz, H. Padmore, A. Young, and A. Scholl, Appl. Phys. Lett. **90**, 162503 (2007).

[8] A. Melnikov, H. Prima-Garcia, M. Lisowski, T. Gießel, R. Weber, R. Schmidt, C. Gahl, N. M. Bulgakova, U. Bovensiepen, and M. Weinelt, Phys. Rev. Lett. **100**, 107202 (2008).

[9] J. Kim, K. Lee, J. Jeong, and S. Shin, Appl. Phys. Lett. **94**, 192506 (2009).

[10] B. Koopmans, G. Malinowski, F. Dalla Longa, D. Steiauf, M. Fähnle, T. Roth, M. Cinchetti, and M. Aeschlimann, Nature Mater. **9**, 259 (2010).

[11] M. Wietstruk, A. Melnikov, C. Stamm, T. Kachel, N. Pontius, M. Sultan, C. Gahl, M. Weinelt, H. A. Dürr, and U. Bovensiepen, Phys. Rev. Lett. **106**, 127401 (2011).

[12] A. Kirilyuk, A. V. Kimel, and T. Rasing, Rev. Mod. Phys. **82**, 2731 (2010).

[13] J. L. Erskine and E. A. Stern, Phys. Rev. B **8**, 1239 (1973).

[14] P. Karri, A. Puri, and J. Tang, IEEE Trans. Magn. **32**, 4099 (1996).

[15] A. R. Khorsand, M. Savoini, A. Kirilyuk, A. V. Kimel, A. Tsukamoto, A. Itoh, and T. Rasing, Phys. Rev. Lett. **110**, 107205 (2013).

[16] C. D. Stanciu, A. Tsukamoto, A. V. Kimel, F. Hansteen, A. Kirilyuk, A. Itoh, and T. Rasing, Phys. Rev. Lett. **99**, 217204 (2007).

[17] T. A. Ostler, R. F. L. Evans, R. W. Chantrell, U. Atxitia, O. Chubykalo-Fesenko, I. Radu, R. Abrudan, F. Radu, A. Tsukamoto, A. Itoh *et al.*, Phys. Rev. B **84**, 024407 (2011).

[18] A. Mekonnen, M. Cormier, A. V. Kimel, A. Kirilyuk, A. Hrabec, L. Ranno, and T. Rasing, Phys. Rev. Lett. **107**, 117202 (2011).

[19] R. Medapalli, I. Razdolski, M. Savoini, A. R. Khorsand, A. Kirilyuk, A. V. Kimel, T. Rasing, A. M. Kalashnikova, A. Tsukamoto, and A. Itoh, Phys. Rev. B **86**, 054442 (2012).

[20] A. Hrabec, N. T. Nam, S. Pizzini, and L. Ranno, Appl. Phys. Lett. **99**, 052507 (2011).

[21] P. Chaudhari, J. J. Cuomo, and R. J. Gambino, Appl. Phys. Lett. **22**, 337 (1973).

[22] S. S. Jaswal, D. J. Sellmyer, M. Engelhardt, Z. Zhao, A. J. Arko, and K. Xie, Phys. Rev. B **35**, 996 (1987).

[23] P. Hansen, C. Clausen, G. Much, M. Rosenkranz, and K. Witter, J. Appl. Phys. **66**, 756 (1989).

[24] N. H. Duc and D. Givord, J. Magn. Magn. Mater **157**, 169 (1996).

[25] S. H. Aly, J. Magn. Magn. Mater. **232**, 168 (2001).

[26] I. Radu, K. Vahaplar, C. Stamm, T. Kachel, N. Pontius, H. A. Dürr, T. A. Ostler, J. Barker, R. F. L. Evans, R. W. Chantrell *et al.*, Nature (London) **472**, 205 (2011).

[27] R. Ahuja, S. Auluck, B. Johansson, and M. S. S. Brooks, Phys. Rev. B **50**, 5147 (1994).

[28] E. Beaurepaire, M. Maret, V. Halté, J.-C. Merle, A. Daunois, and J.-Y. Bigot, Phys. Rev. B **58**, 12134 (1998).

[29] See Supplemental Material at http://link.aps.org/supplemental/10.1103/PhysRevB.87.180406 for more information on the 4T model and calculation parameters.